



## Research papers

# Using cloud computing techniques to monitor long-term variations in ecohydrological dynamics of small seasonally-flooded wetlands in semi-arid South Africa

Siyamthanda Gxokwe<sup>\*</sup>, Timothy Dube, Dominic Mazvimavi, Michael Grenfell

*Institute for Water Studies, Department of Earth Science, University of the Western Cape, Private bag X17, Bellville, 7535 Cape Town, South Africa*

## ARTICLE INFO

This manuscript was handled by S Sally Elizabeth Thomson, Editor-in-Chief

## Keywords:

Artificial intelligence  
Dryland wetland  
Ephemeral wetland  
Machine learning algorithm  
Wetland condition  
Wetland management

## ABSTRACT

Wetlands in drylands have high inter- and intra-annual ecohydrological variations that are driven to a great extent by climate variability and anthropogenic influences. The Ramsar Convention on Wetlands encourages the development of frameworks for national action and international cooperation for ensuring conservation and wise use of wetlands and their resources at local, national and regional scales. However, the implementation of these frameworks remains a challenge. This is mainly due to limited availability of high-resolution data and suitable big data processing techniques for assessing and monitoring wetland ecohydrological dynamics at large spatial scales, particularly in the sub-Saharan African region. The availability of cloud computing platforms such as Google Earth Engine (GEE) offers unique big data handling and processing opportunities to address some of these challenges. In this study, we applied the GEE cloud computing platform to monitor the long-term ecohydrological dynamics of a seasonally flooded part of the Nylsvley floodplain wetland complex in north-eastern South Africa over a 20-year period (2000–2020). The specific objectives of the study were 1) to evaluate wetland ecohydrological dynamics using the 20-year multi-date Landsat composite data coupled with the Random Forest machine learning algorithm, and 2) to establish the major drivers of wetland ecohydrological changes, using selected spectral indices (i.e. Normalised Difference Vegetation Index (NDVI), Normalised Difference Water Index (NDWI) and Normalised Difference Phenology Index (NDPI)) coupled with climate data. The ecohydrology of the wetland changed over time, with some classes increasing twice when compared to the previous measurement, while others decreasing significantly during the study period. Notably, the bare surface class increased at rates of 230% and 350% between 2006–2010 and 2016–2020, respectively. Moreover, the indices showed similar trends throughout the 20-year period, with NDWI having minimum values less than zero in all cases. This implied no surface inundation, although the presence of some wetland vegetation indicated seasonal to semi-permanent soil saturation conditions. A comparative analysis of climate data and remotely sensed indices showed that annual changes of precipitation and evapotranspiration were the main drivers of wetland ecohydrological variations. The findings of the study underscore the relevance of cloud computing artificial intelligence techniques, and particularly the GEE platform, in evaluating wetland ecohydrological dynamics for semi-arid southern African systems which are deteriorating due to the unsustainable use and poor management resulting from limited knowledge about their changes over time.

## 1. Introduction

Semi-arid areas commonly host small intermittently flooded wetlands, which are highly sensitive to climate variability and anthropogenic influences (Wetlands in Dry Lands Research Network, 2014). Anthropogenic influences and climate variability are the major causes of the high inter- and intra-annual ecohydrological variability in these

systems. In many cases, the disappearance of surface inundation during the dry season makes such wetlands susceptible to habitat destruction and loss (Blanckenberg et al., 2020). Globally, semi-arid wetlands have been reported to be declining at alarming rates mostly due to erratic rainfall, climate change and high utilisation by the surrounding communities (Thamaga et al., 2021). In Ethiopia, which is predominantly arid, reports indicate that several seasonal wetlands have been lost

<sup>\*</sup> Corresponding author.

E-mail address: [3050512@myuwc.ac.za](mailto:3050512@myuwc.ac.za) (S. Gxokwe).

(Bahilu and Tadesse, 2017). This has been attributed to unregulated use and over-utilization of these systems resulting in negative impacts on wetland condition. In China, it has been reported that over 30% of wetlands have been lost during the past 50 years due to anthropogenic activities (Liu et al., 2017). Estimates of wetland loss in South Africa range from 50 to 58%, but the full extent of transformation is difficult to quantify over the large spatial scales necessary for informing national policy responses (van Deventer et al., 2019a,b). There is therefore an urgent need for interventions to halt further degradation of these important ecosystems.

In order to sustain these systems, programmes such as the South African National Biodiversity Assessment (van Deventer et al., 2019a,b) and Working for Wetlands (Dini and Bahadur, 2016) are promoting conservation, wise use and restoration of all wetlands at local, national and regional scales. There are also several regional and international efforts aimed at reversing wetland degradation through dissemination of information and involvement of local communities in the establishment of proper management plans (Rebelo, 2010). These efforts are however, hindered by the lack of data on wetland ecohydrological dynamics at appropriate spatial and temporal scales, particularly in the sub-Saharan African region (Gxokwe et al., 2020; Thamaga et al., 2021).

Projects such as the current Wetland Monitoring and Assessment Services for Transboundary Basins in Southern Africa (WeMAST) funded by European Union – Africa Global Monitoring for Environmental Security (EU Africa GMES) have been initiated to ensure the effectiveness of monitoring and assessment of wetlands, using Earth observation data. Such data provide opportunities for producing detailed wetland inventories and understanding wetland dynamics at scales relevant to the management of wetlands of varying sizes (e.g. van Deventer et al., 2019a,b). Moreover, the availability of cloud computing platforms such as Google Earth Engine (GEE) supports efforts of regional wetland analyses, using Earth observation data. The availability of 40 years and over a petabyte of remotely-sensed data that are freely accessible, coupled with advanced machine learning algorithms on the GEE platform, makes it possible to consistently monitor small to large wetlands and track their changes over-time (Gorelick et al., 2017). This therefore provides the necessary baseline information about ecohydrological dynamics that is much needed for developing management actions.

Although the GEE cloud computing platform offers numerous advantages to address issues of limited and inconsistent data for wetland monitoring, the utility of this platform in monitoring long-term changes in the ecohydrological dynamics of semi-arid wetlands requires further evaluation (Wua et al., 2019). Studies that have utilized this platform for long-term monitoring of environmental change include mapping of forests, croplands and open water (Kumar and Mutanga, 2018; Tamiminia et al., 2020). The most recent studies which have utilized GEE in wetlands mapping have demonstrated the potential value of this platform in wetland studies (Gxokwe et al., 2021; Zhou et al., 2019). Although these studies underscore the relevance of utilizing GEE for investigating small seasonally-flooded wetlands, they did not assess longer-term changes using time-series data in GEE.

There is therefore a need to assess the applicability of the GEE and multi-source spatial data in monitoring long-term changes in ecohydrological dynamics of wetlands in semi-arid environments, particularly in sub-Saharan Africa. This will aid in developing consistent and comparable wetland inventories and assessments across the region, and advance an understanding of drivers of wetland dynamics (including anthropogenic stressors that contribute to wetland degradation and loss). This will enhance local, regional and international wetland conservation and management programmes. Moreover, long-term monitoring of ecohydrological dynamics is critical for preventing or managing loss of wetland ecosystem services (Millennium Ecosystem Assessment, 2005). The current study therefore aims to assess the utility of the GEE cloud computing platform for monitoring long-term variations in ecohydrological dynamics of small seasonally-flooded wetlands in a semi-arid region of South Africa over a 20-year period (2000–2020),

using Nylsvley floodplain as a case study. The specific objectives are 1) to evaluate the spatio-temporal variations in ecohydrological dynamics of wetlands using time-series Landsat composite data coupled with GEE machine learning algorithms, and 2) to establish the major drivers of ecohydrological changes in the studied systems using remotely sensed metrics coupled with climate data.

## 2. Study area

The study was conducted on part of the Nylsvley floodplain located within the Limpopo Transboundary River Basin (LTRB) (Fig. 1a) in the Limpopo Province (Fig. 1b), South Africa. The Nylsvley floodplain is 70 km long and 7 km wide when fully inundated bordering the Nyl River (see the dotted line in Fig. 1c) (24.632116 °S and 28.684779°E; 24.614213°S and 28.686909°E, 24.659827°S and 28.692914°E; 24.659699°S and 28.696835°E). This floodplain is a Ramsar-listed wetland (Dzurume et al., 2021) and derives water from the Olifants-spruit, Groot and Klein Nyl rivers, during the period of high flows (September to December) as well as local rainfall (Botai et al., 2020; Dzurume et al., 2021; Mosase et al., 2019). The dominant vegetation includes short grass species such as *Cynodon dactylon* (Bermuda grass) and *Oryza longistaminata* (rice grass) and long grass species such as *Phragmites australis* (common reeds). Other plant species present include *Vachellia tortilis*, *Vachellia nilotica* and *Vachellia karoo* (African Conservation, 1998). The Nylsvley floodplain serves as an important habitat for about 80 000 birds when inundated (Vlok et al., 2006). The study focused on the protected area within the Nylsvley Nature Reserve covering an area of 13.69 km<sup>2</sup> (Fig. 1c).

## 3. Materials and methods

### 3.1. Field data collection

Field data were collected between 28-09-2020 and 1-10-2020. A total of 300 ground truth points representing different landcover classes were collected during field surveys, using a handheld Geographical Positioning System (GPS) with an error margin of less than 3.65 m. The landcover observed during field surveys included classes such as bare surfaces, short wetland grass species comprising of *Cynodon dactylon* (Bermuda grass) and *Oryza longistaminata* (Rice grass), as well as long wetland grass species comprising of only *Phragmites australis* (Common reeds). These vegetation communities were visually identified in the field. The floodplain was completely dry during the field survey and therefore no water surface was identified. The field survey period coincided with the months when some of the images used in this study were acquired. Ground truth points were collected following a stratified random sampling approach. Consequently, the floodplain was subdivided into 30 m × 30 m quadrants which were spaced by about 10 m apart. The 30 m × 30 m quadrants were chosen because of the pixel sizes of the remotely sensed data used as well as the size of the studied floodplain. This is supported by a number of remote sensing studies such as Mudereri et al., (2021); Thamaga and Dube, (2018). A minimum of 20 points were randomly collected from each quadrant depending on the heterogeneity of the landcover identified in each quadrant and the accessibility of some sections within the wetland. The field data were further supplemented by 350 additional points that were randomly extracted from higher resolution Google Earth images, coinciding with dates of some of the remotely sensed images used. The data gathered from field visits and higher resolution Google Earth image comprised of 552 points representing short grass species, 68 points for bare surface and 30 points for long grass species. The collected points were then randomly split on R-studio into 70% for training (386 points for short grass, 48 points for bare surface and 21 points for long grass) and 30 % for validation (136 points for short grass, 20 points for bare surface and 9 points for long grass) of classification of images by the Random Forest model.

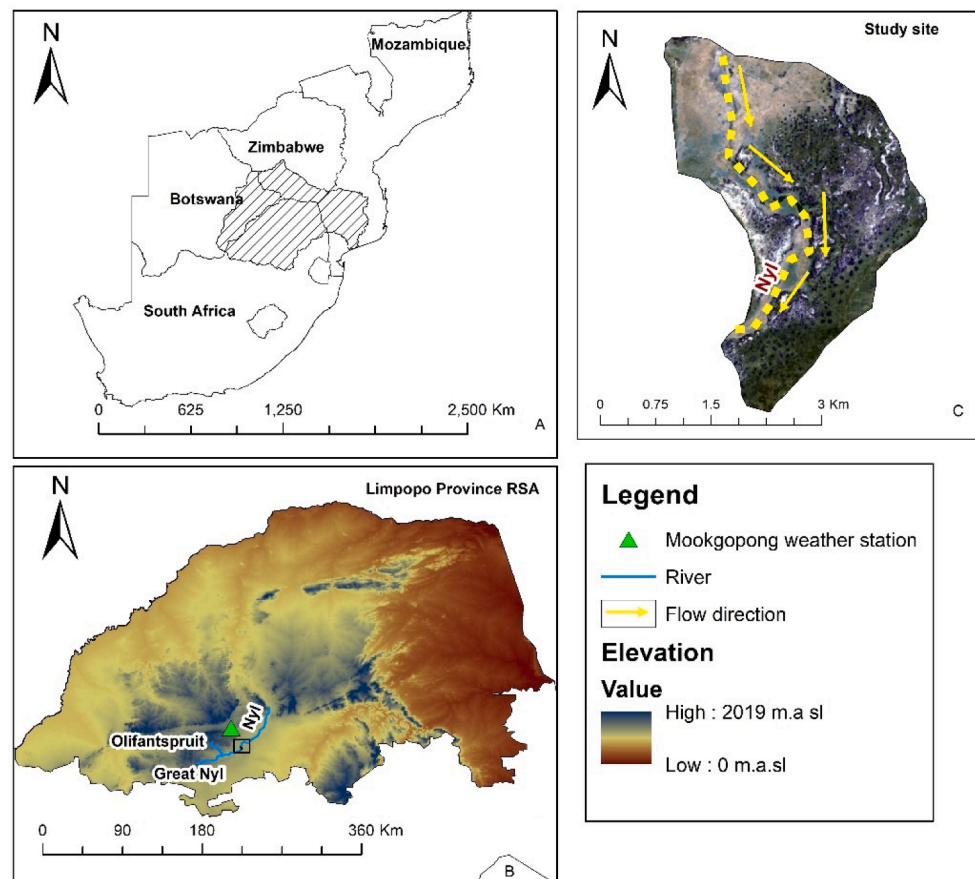


Fig. 1. Location of the Nylsvley floodplain. The map of the floodplain was produced using a true colour composite of a Sentinel-2 image captured on the 15th October 2020.

### 3.2. Ancillary data

The 2000–2020 monthly rainfall and temperature data for the Mookgopong Weather Station located at  $-24.42745$  and  $28.59419$  North West of Nylsvley floodplain were collected from the South African Agricultural Research Council. The station is located at an altitude of 820 m towards higher elevation areas, and 26 km away from the studied floodplain (Fig. 1c). Due to the unavailability of evapotranspiration data, evapotranspiration rates were estimated using the following Hargreaves and Samani, (1985) equation (1):

$$E = 1.25 \times 0.0023 \times R_a T_r^{0.5} (T_a + 17.8) \quad (1)$$

where  $E$  is potential evapotranspiration rate (mm/day),  $R_a$  is extra-terrestrial radiation (mm equivalent per day),  $T_r$  is monthly temperature range ( $^{\circ}C$ ) and  $T_a$  is average daily temperature for the month ( $^{\circ}C$ ). Other methods for estimating evapotranspiration such as the Penman-Monteith equation could not be used because solar radiation, wind speed and relative humidity are not available for the study area.

### 3.3. Remote sensing data acquisition and processing

The steps followed during the acquisition and processing of remote sensing data are presented in Fig. 2. Prior to image classification, remotely sensed products were extracted from the GEE catalogue. The images extracted are for the Landsat-7 ETM+ chosen because of having the longest availability on the platform. Although it is reported in the literature that Landsat-7 ETM+ was adversely affected by the failure of the Scan Line Corrector SLC (Dube and Mutanga, 2015) after 31 May 2003, the stripes caused by this failure did not affect the area covered by

the studied wetland. The data collected was then filtered by the boundaries of the studied wetland and the date, using the codes “Image.filterBounds ()” and “ee.Filter.Date ()” in the GEE cloud computing platform. After filtering of images by dates and boundaries, they were then filtered by cloud cover. Images with clear cloud coverage (0%) were selected because of the size ( $13.69 \text{ km}^2$ ) of studied wetland. Images with cloud cover were excluded since cloud masking would result in severe error propagation. The “ee.Filter.eq (“CLOUD\_COVER”, 0)” code was used to filter images with clear cloud cover. The number of images obtained from the filtering process are presented in Table 1. Cloud free images were then grouped by intervals of 5 years. The first interval was from 2000 to 2005 and all the images for that period were grouped. The second and third intervals were from 2006–2010 and 2011–2015, and the last interval was from 2016 to 2020. After the grouping of images, wetland indices such as the Normalised Difference Vegetation Index (NDVI), Normalised Difference Water Index (NDWI) and Normalised Difference Phenology Index (NDPI) were computed for all images obtained in each interval using the equations presented in the supplementary material (Table A) then extracted to assess their variations overtime. These indices were used as proxy for ecohydrological dynamics. The NDVI was chosen because of its sensitivity to photosynthetically active biomass, which enables discrimination between wetland and non-wetland areas as well as vegetated and non-vegetated areas (Liu and Huete, 1995). NDWI was chosen as this can discriminate between water and non-water areas. Although it was noted that the studied system has very limited open water, the NDWI was used to capture pixels which may have open water at any time periods. NDPI which was recently developed by Wang et al., (2017) and it uses the weighted combination of Red and Short-Wave Infrared (SWIR) bands instead of the red band like in the NDVI. The weighted combination is

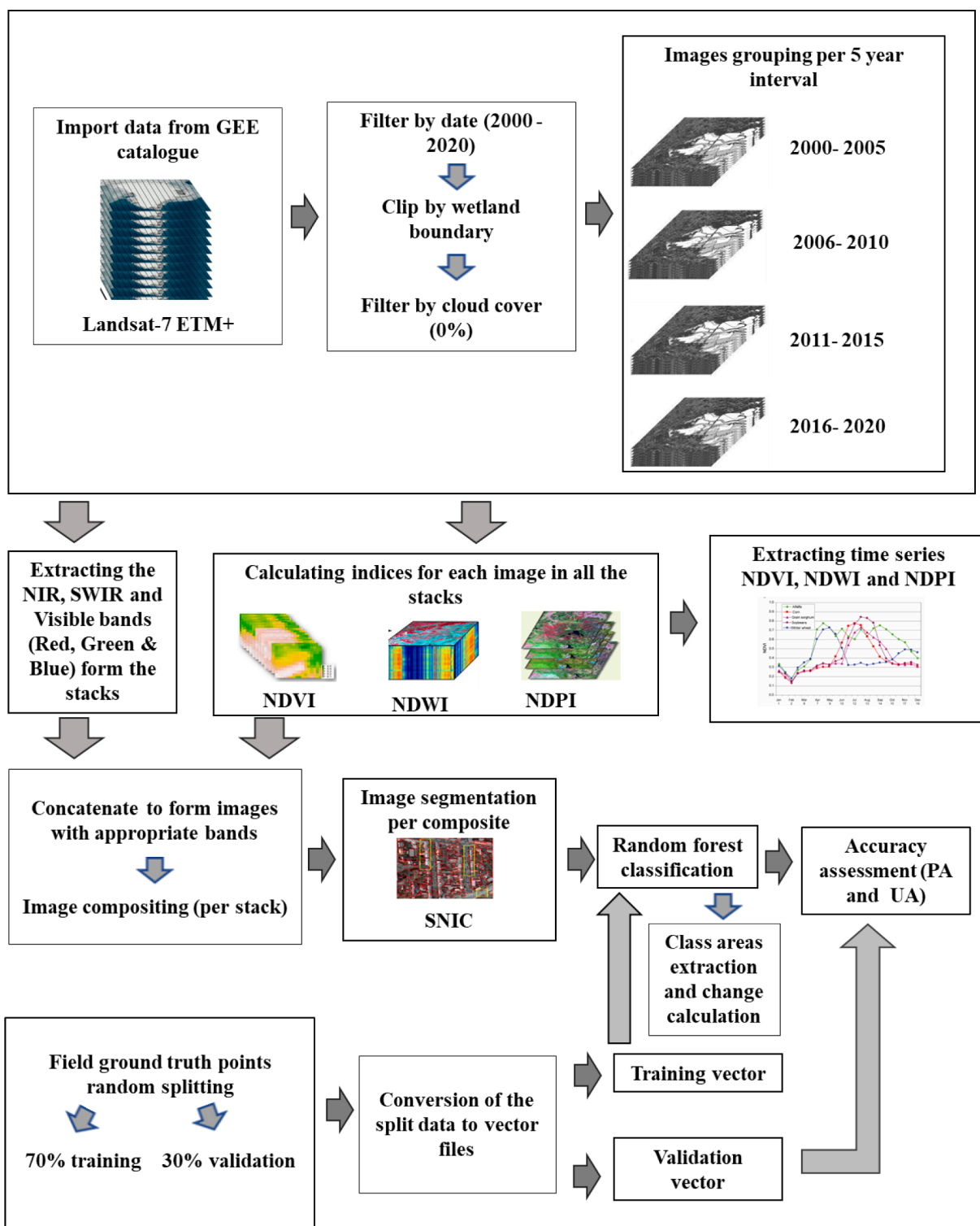


Fig. 2. Image classification process using the GEE cloud computing platform.

Table 1

Number of remotely sensed images with no cloud cover obtained per time intervals with their details.

Period	No. of images obtained	Remote sensing product
2000–2005	26	Landsat (ETM+)
2006–2010	20	Landsat (ETM+)
2011–2015	25	Landsat (ETM+)
2016–2020	37	Landsat (ETM+)

almost equal to the value of Near Infrared band (NIR) for different soils and is sensitivity to vegetation. Moreover, the NDPI considers the absorption of leaf water content in the SWIR band, thus could account for variations in canopy water content. This assist in improving the separability of soil and vegetation with varying leaf water content- a previous daunting task when using NDVI. The NDPI was chosen for these reasons. Further, the above-mentioned indices were computed from the time series data and then used to assess wetland ecohydrological dynamics overtime. In addition, visible (Red, Green and Blue), NIR and

SWIR bands were extracted from the grouped images representing each interval, and concatenated to the extracted indices to form images with only the appropriate band combinations that better enhances the wetland features. The concatenated images were then composited per interval to form single images representing each interval using the median composite algorithm in GEE. The median composite algorithm reduces a stack of images by calculating a median across the matching bands of the image stack thus minimising the illumination effects such as shades as well as the effects of cloud cover (Gorelick et al., 2017; Mahdianpari et al., 2020). Consequently, the derived composite images were subjected to the Object Based Image Analysis (OBIA). OBIA was chosen because of its superiority to pixel-based analysis. Various studies such as Mahdianpari et al., (2019); Pande-Chhetri et al., (2017), have shown that OBIA does not only rely on spectral characteristics but also considers contextual information (height, texture, area, perimeter etc.) of a pixel which helps in improving the discrimination of wetland classes. The initial step in OBIA, is image segmentation. This process involves the partitioning of the image into multiple discrete and non-overlapping objects based on a specific criterion. This maximizes the separability of different landcover classes and prevents the “salt and pepper” effects on the final classified image (Dlamini et al., 2021a). Further, a Simple Non-Iterative Clustering (SNIC) Algorithm was used to partition the composite images. The SNIC undertakes image segmentation by initializing the centroids in a regular gridded image, and then the dependency of each pixel relative to the centroids is established, using the distance in five-dimensional space of colour and spatial coordinate. The distance joins the normalised spatial and colour distances to produce uniform super pixel. The candidate pixel is added to the cluster based on its shortest distance to the centroid (Achanta and Süssstrunk, 2017). The algorithm was selected because of the simplicity, memory efficiency as well as the ability to incorporate connectivity between the pixels after initiation of the algorithm. The SNIC algorithm was implemented using the code “ee.Algorithms.Image.Segmantation.SNIC()” and the outputs were images with super pixels as well as contextual information of those pixels such as areas, texture (standard deviation), perimeters and heights. These were then integrated with the selected spectral bands and used as an input concatenate images in the selected machine learning algorithm.

### 3.4. Adopted wetland classification approach

Classification of the acquired images was executed using the Random Forest (RF) Machine Learning Algorithm in the GEE cloud computing platform. The RF algorithm is an ensemble non-parametric classifier which consists of many different trees from subsets of randomly selected training data (Dlamini et al., 2021b). Each tree casts a unit vote to decide on the final class of the object. The algorithm was selected because of the ability to handle large differences between landcover classes, thereby neutralising noise in the data set (Simioni et al., 2020). Moreover, the selection of the RF algorithm in this study was informed by a study by Gxokwe et al., (2021) which identified RF as an appropriate GEE algorithm for classifying small seasonally-flooded wetlands. Comparatively, the RF algorithms produced highest overall, producer’s and user’s accuracy. Prior to the classification, the ground truth points were split on R-studio into 70% training and 30% validation samples. The split training data were then imported and converted to vector files in a GIS environment, and then imported to the GEE to train the classifier. The training of the RF classifier on GEE was executed using the code “ee.Classifier.train()”. In training the object-based RF model, the grid search value for *mtry* parameter was varied from 1 and 5. The grid search value for *ntree* parameter was varied from 500 to 10 000 with an interval of 500. The ranges were selected based on studies of similar nature such as Dlamini et al. (2021a,b); Gxokwe et al., (2021); Ryan et al., (2014). The search yielded hundred combinations of *mtry* and *ntree* values, and the optimum values (1500 *ntree* and 5 *mtry*) from these combinations were finally used as the RF model input parameters for classifying the

Landsat-7 composite images. Classification of the remotely sensed image composites was then executed using the code “Image.classify()”.

### 3.5. Accuracy assessment

Accuracy assessment was executed using three metrics namely, the Overall Accuracy (OA), User’s Accuracy (UA) and Producer’s Accuracy (PA). OA measures the overall correctly classified pixels (Story and Congalton, 1986) and UA measures the probability that a classified pixel of a particular category belongs to that category on the ground. PA measures how well the reference ground cover type pixels were classified (Story and Congalton, 1986). The OA was implemented using the code “Image.accuracy()” in GEE. PA and UA were implemented using the codes “Image.producersAccuracy” and “Image.consumersAccuracy()”. During the implementation of the above-mentioned algorithms in GEE, the validation vector produced from the 30% field data was firstly imported to the platform, and zones on the classified image corresponding to the vector points were sampled using the code “Image.sampleRegions()”. The sampled zones as well as the validation vector points were then used as input files to the latter algorithms to compute each accuracy metric (OA, UA and PA).

### 3.6. Change analysis, variations and major drivers

To assess wetlands ecohydrological changes, the area covered by each land cover class were estimated from the classified image per interval and the rate of change for each class (RAC) was established using the method described by Shen et al., (2019) (Equation (2)).

$$RAC = \left( \frac{EA - IA}{IA} \right) \times 100\% \quad (2)$$

where RAC is given as the rate of change of wetland area; EA is the area at the of the period considered (refers to the areas in years 2000–2005, 2006–2010, 2011–2015, 2016–2020); IA is the initial wetland area (refers to the total area for the period of 2000–2005 calculated as the sum of the surface areas covered by the wetland classes identified). The variations in ecohydrological dynamics were established by analysing time series of NDVIs, NDWIs and NDPIs which were used as proxy for wetland ecohydrological dynamics.

## 4. Results

### 4.1. Variations in ecohydrological dynamics

The changes in spatial distribution of the wetland cover classes for the time periods are presented in Fig. 3. Water class could not be identified using the object-based RF model due to unavailable training and validation data for this class. This is resulting from no visible spatial coverage of the class during the ground truthing period, which may have been caused by short term surface inundation. Moreover, the indices used could not detect any water class mainly because of the forested vegetation within the wetland, as well as the spatial resolution of the data used. Although water could not be detected, most vegetation species identified such as *Phragmites australis* are associated with the presence of semi-permanent saturated wetland soils which provided ecohydrological information about the Nylsvley floodplain. This is supported by the findings in Kotze and O’connor, (2000), who reported that species such as *Phragmites australis* were associated with wettest zones within the studied wetland, therefore implying that ecohydrology information could be deduced from these types of species.

The class distribution shows that the short grass was the most dominant class except for the period 2016 to 2020 when bare surface was the most dominant class. Long grass was the least dominant class for all the cases except for the 4th period (2016–2020) where short grass was least dominant. Visual assessment of the changes from the derived

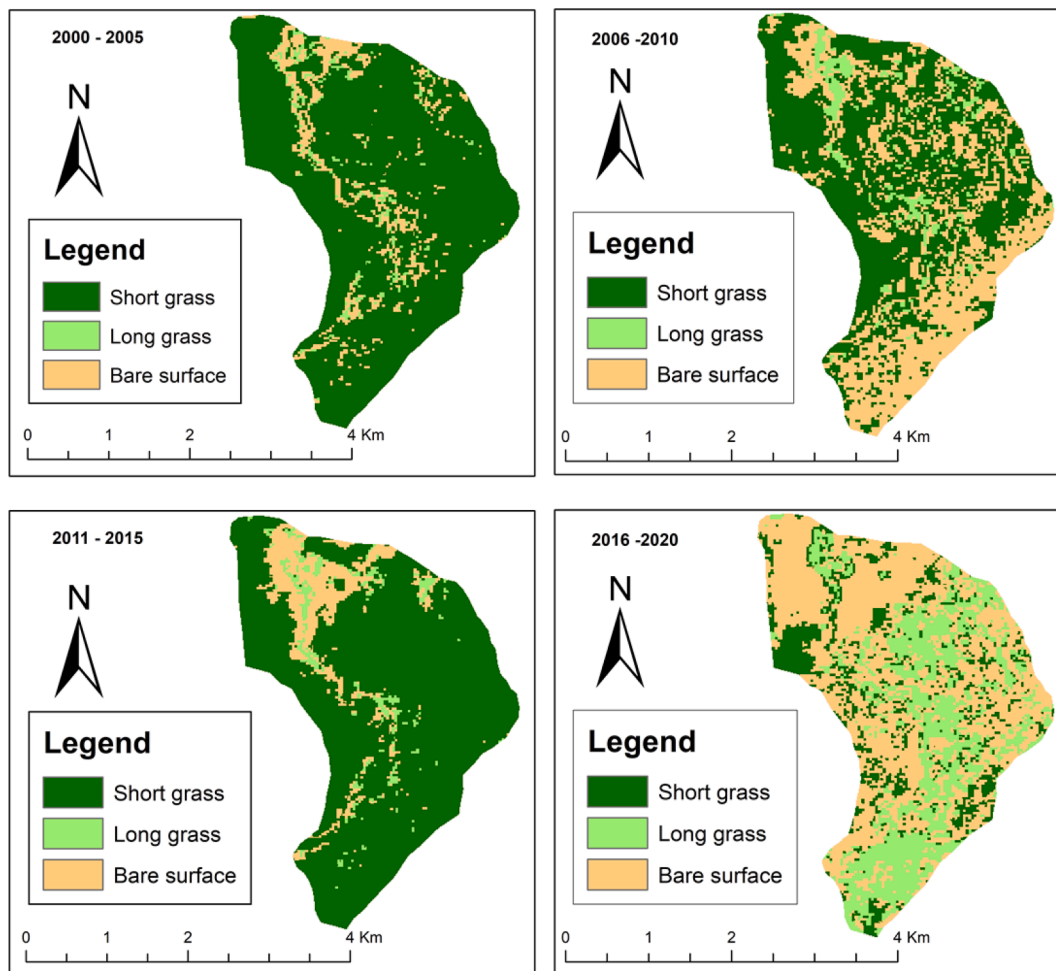


Fig. 3. Spatial distribution of wetland classes for the studied periods (Period 1: 2000–2005, Period 2: 2006–2010, Period 3: 2011–2015 and Period 4: 2016–2020), produced using object based Random Forest classification of Landsat-7 data.

spatial distribution maps of the wetland classes shows variations in these classes over time. These results show that classes such as short grass and long grass declined between period 1 and 2 (2000–2005 and 2006–2010). However, a resurgence was observed in these classes

during period 3 (2011–2015). For bare surface an increase was noted for the entire monitoring period except for period 3 (2011–2015) where a decline of about 1.5 km<sup>2</sup> was noted. A sharp decline in spatial distributions of short and long grass were observed for the period 4

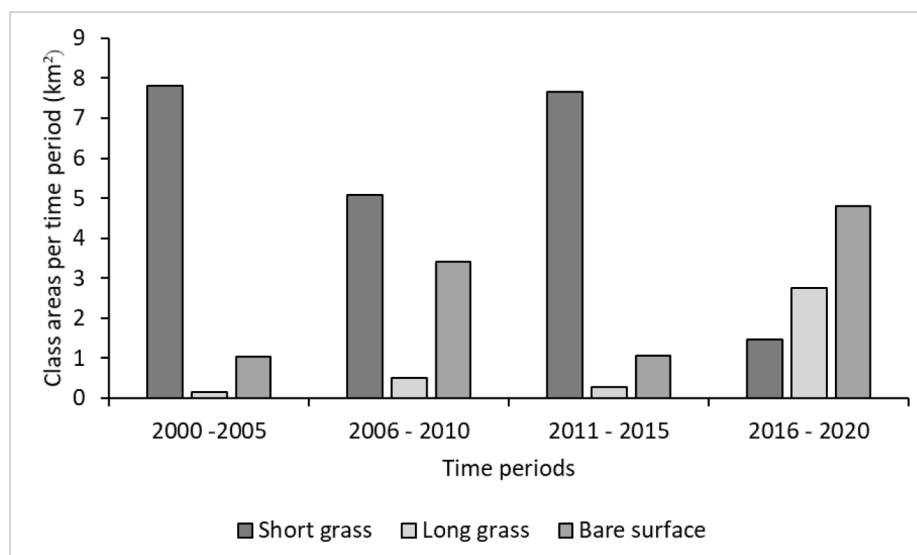


Fig. 4. Nylsvley floodplain land cover surface areas per time periods (Period 1:2000–2005, Period 2: 2006–2010, Period 3:2011–2015 and Period 4: 2016–2020).

(2016–2020) as bare surface sharply increased for the same period.

The class area results shown in Fig. 4 corroborate with the visual observation during fieldwork of the spatial distribution of the identified wetland classes. The results show that the short grass class had the highest surface area for the periods 1, 2 and 3 (2000–2005, 2006–2010 and 2011–2015), with surface areas ranging between 5 km<sup>2</sup> and 8 km<sup>2</sup>, respectively. The long grass had the lowest surface area for the above-mentioned periods, which ranged between 0.1 km<sup>2</sup> to 0.5 km<sup>2</sup>, respectively. During period 4 (2016–2020), bare surface had the highest surface area of 4.8 km<sup>2</sup> and short grass had the lowest (1.5 km<sup>2</sup>).

The results on the rate of change per class are shown on Table 2. Drastic changes occurred in the wetland cover classes at high rates between the periods. The results show that the short grass declined at a rate of about 38% between the period 1 and 2 (2000–2005 and 2006–2010), whereas other classes increase at a rate of 228% and 230%, particularly bare surface, which doubled compared to period 1 (2000–2005). Although a decline in short grass was observed for the above-mentioned periods, there was an increase in this class during the period 3 (2011–2015) at a rate of 51%. Bare surface and long grass decreased at the rates of 69% and 46% respectively for period 3 (2011–2015). Furthermore, the results show that the short grass declined by 81%, while other classes such as long grass doubled.

There were no major changes of the temporal variations of NDVI, NDPI and NDWI for the Nylsvley floodplain (Supplementary material: Figure A). However, the NDWI had low values less than 0 throughout implying that there was no surface inundation detected. NDPI and NDVI had values greater than 0 in most cases particularly for the time periods 2000–2005, 2006–2010 and 2016 – 2020 (supplementary material: Figure A) implying that there was vegetation detected although it was not healthy.

#### 4.2. Accuracy assessment

The accuracy assessment results showed that the OA (Fig. 5) for all the periods were within the acceptable range between 72 % and 78%, with 2011 – 2015 and 2016 – 2020 having the highest values and 2006 – 2010 the lowest value.

The class accuracy results are presented in Table 3. The results show that for all the periods the PA ranged between 33% and 88%, and the short grass had the highest PA in all the cases and long grass had the lowest PA particularly for period 1 and 2 (2000–2005 and 2006–2010), during which the PA was 33%. For period 3 and 4 (2011–2015 and 2016–2020), the bare surface had the lowest PA with 37.5% for both periods. The UA results ranged from 40% to 100% with long grass having the highest UA for period 1 and 2 (2000–2005 and 2006–2010). The lowest UA was for bare surface during period 1 (2006 – 2010) with a proportion of 40% (Table 3).

#### 4.3. Drivers of ecohydrological variation

A statistical summary of the NDVI, NDWI and NDPI results for all the periods are presented in the supplementary material (Figure B). The results indicate that the indices are mostly positively skewed except for NDWI for years like 2006 in time period 2 and 2014 in time period 3,

**Table 2**  
Rate of change of Nylsvley floodplain between the time periods.

Class	Rate of change from P1 to P2 (%)	Rate of Change from P2 to P3 (%)	Rate of Change from P3 to P4 (%)
Short grass	–38	51	–81
Long grass	228	–46	896
Bare surface	230	–69	350

\*P1: 2000–2005, P2: 2006–2010, P3: 2011–2015 & P4: 2016–2020.

which have symmetric distributions. The data also show larger variations in most cases with large ranges (stretched whiskers), except for some years such as 2003 in Period 1 (2000–2005), where the whiskers for NDVI, NDWI and NDPI are squeezed, as well as 2008 and 2009 in Period 2 (2006–2010), where the whiskers are short. The outliers were observed for NDVI, NDWI and NDPI data for the year 2004 in time period 1 and in period 4 for the years 2017, 2018 and 2019. For the time period 3, outliers were observed for NDVI during the year 2015. Further, an inverse relationship between the biomass (indices) and the annual ET rate (Fig. 6) was noted. The NDPI decreased considerably during years when ET increased, e.g. 2002 and 2004 (Fig. 6a).

The biomass indices except for NDPI tended to increase as expected with the amount of annual precipitation, e.g. 2007 to 2009 (Fig. 7). This relationship is however not evident during some years such as 2002 to 2004 in time period 1. A wetland typically stores both surface and subsurface water, and therefore a decrease in rainfall in a single year such as 2002 and 2003 may not have significant effects to the growth of plants as they may be utilising water already in storage.

## 5. Discussion

This study assessed the utility of the GEE cloud computing platform in monitoring long-term (2000–2020) variations in ecohydrological dynamics of the small seasonally-flooded wetlands in a semi-arid environment of South Africa, using the Nylsvley floodplain as a case study. The main classification results showed that the following three land-cover classes could be identified; i) short grass vegetation characterised by species such as *Cynodon dactylon* and *Oryza longistaminata*, ii) long grass species such as *Phragmites australis*, and iii) bare surfaces. These land cover classes represent zones with semi-permanent soil saturation as shown by the presence of *Phragmites australis*, and temporary to seasonal saturation represented by short grass (*Oryza longistaminata*) (Kotze and O'Connor, 2000). While overall the Nylsvley floodplain may be considered a seasonally flooded system, the results of this study show that the system contains both seasonal and semi-permanent hydro-periods because of the presence of the above-mentioned wetland vegetation species which are viewed as indicators of environments with semi-permanent saturated soils and seasonal inundation. The water class could not be detected due to unavailable training and validation data covering this class resulting from the absence of surface inundation during the period of ground truthing. Moreover, the remotely sensed spectral indices used failed to detect the presence of water mostly due to the dense vegetation in parts of the studied system as well as the spatial resolution of the landsat-7 ETM+, which was selected because of the length of the image record, and the number of good quality images (Table B in supplementary material) available for this product on the GEE catalogue.

Accuracy assessment results showed that an overall accuracy was within the acceptable range of 69% – 79%. Although this was the case, there were some inaccuracies for classes such as bare surface and long grass for some periods. These can be mostly attributed to the spatial resolution of the remotely sensed product used, which resulted in significant spectral mixing between the classes. Several studies such as Dvoretz et al., (2016) and Gxokwe et al., (2021) have demonstrated that the spatial resolution of the remotely sensed data does significantly impact the accuracy of classification results particularly when mapping small areas such as the wetlands studied here. Moreover, the report by Federal Geographic Data Committee (1992) highlighted that with Landsat data which is used in this study, accurate identification of an object requires at least 9 pixels, which covers a total surface area of about 0.9 ha and at most 25 pixels. The limited training data of bare surface and long grass relative to the short grass species due to the spatial coverage of these classes within the wetland led to unequal distribution of training points, which affected the ability of the training data to adequately characterise the classes of interest.

Due to the small size of bare surface and long grass within the

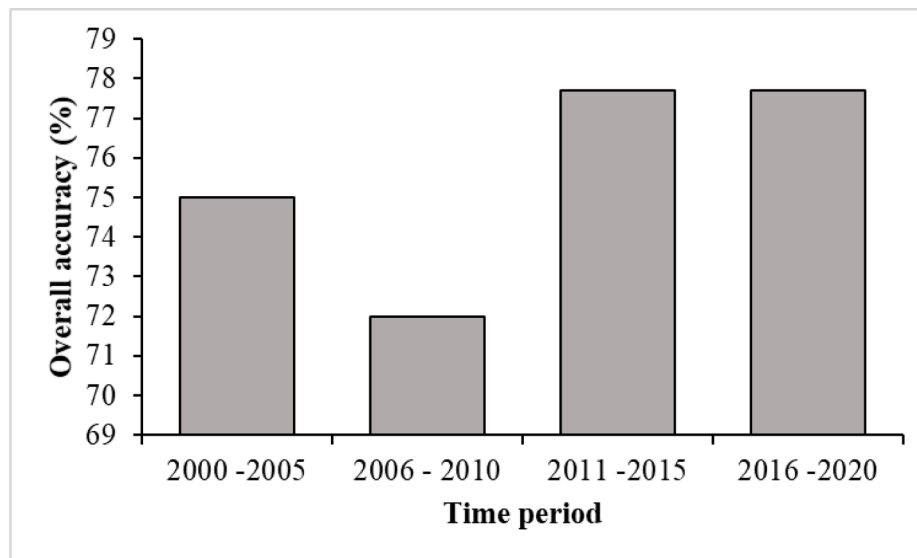


Fig. 5. Overall accuracy for the classified image composites for each period (Period 1: 2000–2005, Period 2: 2006–2010, Period 3: 2011–2015 and Period 4: 2016–2020).

Table 3

Error metrics results for the classified image composites representing the time Period 1: 2000–2005, Period 2: 2006–2010, Period 3: 2011–2015 and Period 4: 2016–2020.

Period	Class	PA (%)	UA (%)
2000–2005	Short grass	88	78.57
	Long grass	33.3	100
	Bare surface	50	57.14
2006–2010	Short grass	84	84
	Long grass	33.3	100
	Bare surface	50	40
2011–2015	Short grass	92	85.18
	Long grass	66.6	66.6
	Bare surface	37.5	50
2016–2020	Short grass	92	88.46
	Long grass	66.6	50
	Bare surface	37.5	50

wetland, fewer points were collected for these classes than for short grass thus resulting in the imbalance in training samples. These imbalances are likely to have caused inaccuracies in the classification of bare surface and long grass than short grass which had more training data. Several studies such as Millard and Richardson, (2013); Ustuner et al., (2016); Xia et al., (2019) have demonstrated that unequal distribution or imbalance in the training data is likely to influence the classification accuracy of the classes in a way that the over-represented classes may dominate the underrepresented classes resulting in classification inaccuracies for the underrepresented classes. However, the imbalances in training samples in this case were not as a result of sampling error but rather a result of lower number of training points available for bare surface and long grass caused by the small areal coverage these land cover class in the area under study.

The spatiotemporal variation results showed that ecohydrological conditions varied from one period to another, denoted by some of the classes changing to more than double, the previous area, and some which significantly dropped to half the previous period. The results indicated that in most cases bare surface significantly increased for periods such as 2006–2010 and 2016–2020. This can be attributed mostly to seasonal changes as most images used for these periods were collected during dry season (addendum A), which is the leaf off season. Few suitable images were available for the wet season images (leaf on season) due to frequent cloud cover. Moreover, below average precipitation

was received in the LTRB around 2016–2017 which significantly impacted most ecosystems including the wetlands in the area (Gxokwe et al., 2021), which therefore explains the cause of bare surface domination. This is also evident in Figure 9. The temporal variations in the indices results showed similar trends between NDVI, NDWI and NDPI and the floodplain was dry for most times. These finding corroborates with Nhamo et al., (2017) who reported high seasonal variabilities in wetland of the Witbank Catchment in South Africa although the study focused only on inundation dynamics at larger scale than the studied.

As expected, there was an inverse relationship between ET and wetland biomass for all the periods. This is because ET tends to contribute to water losses in wetlands, particularly in semi-arid regions, therefore resulting in loss of moisture available in wetlands and thus contributing to the decline in the NDWI values for the wetlands. Due to the decline in moisture content available in the wetland, some vegetation become less healthy because water stress results in NDVI and NDPI decline. A study by Al-Shehhi et al., (2011) monitored the effects of variable soil moisture content to the MODIS derived NDVI for different vegetation species in Abu Dhabi. The findings showed that with increasing evaporation rates, less healthy vegetation dominated the studied area due to plants wilting, thus resulting in decreased NDVI values. These results by Al-Shehhi et al., (2011) corroborate with the findings of current study although the focus was not only on wetland vegetation. Further, West et al., (2018) studied vegetation response to varying soil moisture using Sentinel-2 data, and the results show strong correlation between Sentinel-2 derived NDVI as well as soil moisture content, which therefore supports the findings of the current study.

Comparative analysis of annual precipitation with average NDVI, NDWI and NDPI showed that with increase in annual precipitation the indices also increased for all the time periods except for 2000–2001 where the indices showed delayed response to varying annual precipitation. The delayed response could be resulting from the use of dry season images which corresponds to the leaf off season for vegetation and low flow period for inundation. The study by Chen et al. (2020) evaluated the vegetation response to precipitation anomalies in the semi-arid Inner Mongolia Plateau China over a 34-year period using the Advanced Very High-Resolution Radiometer (AVHRR) derived NDVI and multi-source precipitation data. The findings of the study show that there is a time lag in vegetation response to precipitation though the duration is not visible.

Annual variations of rainfall and evapotranspiration rates have been shown in this study to be major drivers for the ecohydrological dynamics

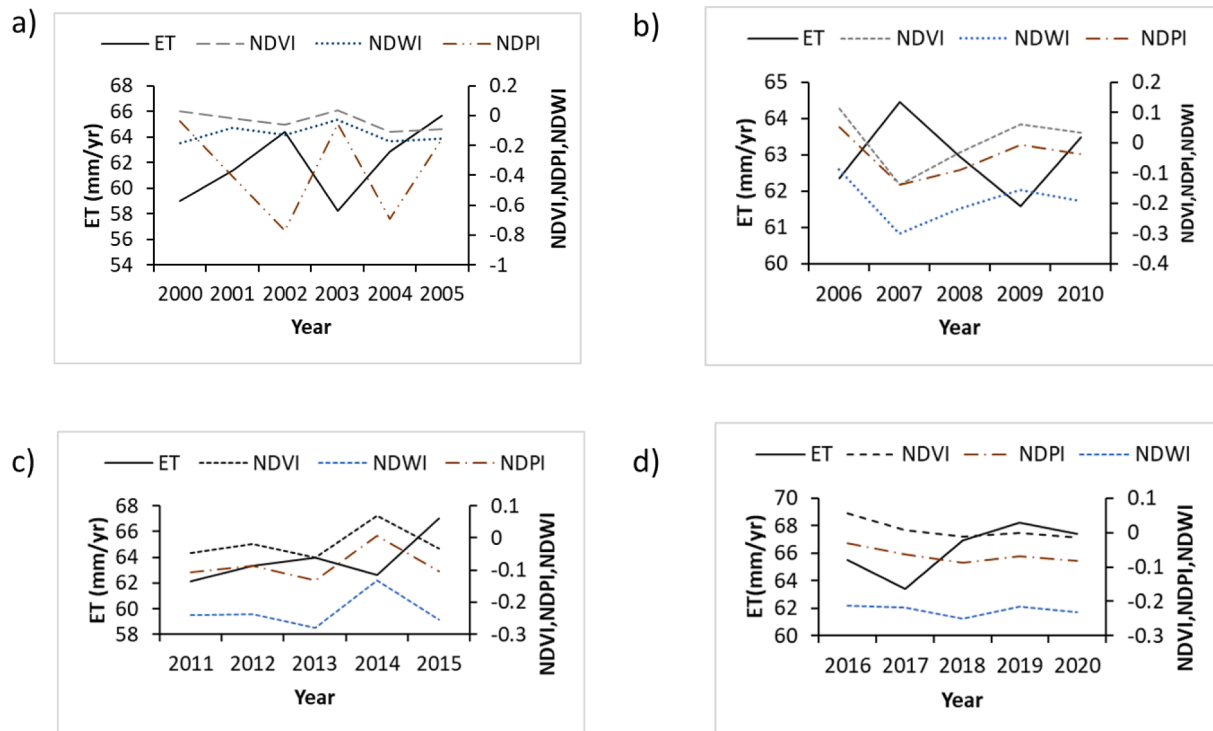


Fig. 6. The relationship between biomass (indices) and annual ET rates for a) Period 1: 2000–2005, b) Period 2: 2006–2010, c) Period 3: 2011–2015 and d) Period 4: 2016 – 2020.

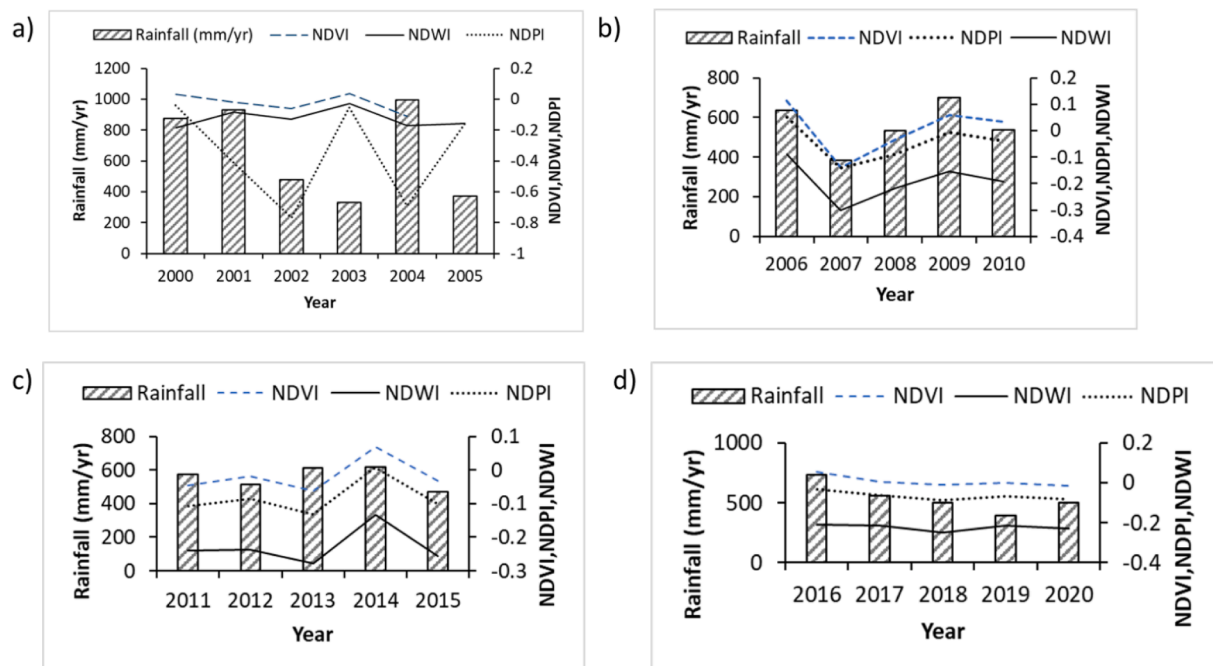


Fig. 7. Comparative analysis of the indices and rainfall data for a) Period 1: 2000–2005, b) Period 2: 2006–2010, c) Period 3: 2011–2015 and d) Period 3: 2016 – 2020.

of the Nylsvley floodplain. Annual rainfall will also influence the availability of both soil water and groundwater which also influence vegetation growth in a wetland. These finding corroborate with the study of Birkhead et al. (2007) which modelled the hydraulic behaviour of the Nylsvley floodplain using field measured climate data coupled with LIDAR data. The study identified ET and annual rainfall as driving factors of the ecohydrological changes in the floodplain.

Overall, the findings underscore the relevance of cloud computing artificial intelligence platforms such as GEE in monitoring long-term variations in ecohydrological dynamics of semi-arid wetlands in the sub-Saharan region, and therefore providing information on their degradation rates and loss which is currently unknown for these regions. These findings are critical in the development of sustainable use and management frameworks of small seasonal flooded wetlands in semi-

arid regions. Besides, they provide useful alternative ways and robust methodologies to generate routine and continuous wetland information about their changes - a previous daunting task from traditional mapping and monitoring techniques. This therefore will aid in development of local to global scale frameworks that will assist in setting up conservation policies and apply effective management practices of wetlands, particularly in data scarce regions with semi-arid climates and semi-permanent wetland with varying ecohydrology that typically may be over exploited during dry periods.

The study also informs the ongoing efforts by the projects such as Global Monitoring Environment and Security (GMES)—Africa hosted by Southern African Science Services Centre for Climate Change and Adaptive Land Management which is promoting the use of Earth observation data for assessing, monitoring and managing wetlands in transboundary basins, to prevent loss of ecosystems services. which are beneficial to the communities around these systems. Further, the study contributes towards achieving the key priority areas of the African Union's Agenda 2063, which elaborates on preserving at least 17% of the of terrestrial and inland waters (including wetlands) and 10% of the marine areas by 2023. The study also contributes to achieving Sustainable Development Goal (SDG 6.6) which advocates for the prevention of the destruction and degradations of all the ecosystems, and rehabilitating those that had already been destroyed (Sudmanns et al., 2020).

## 6. Conclusion

The study utilized remotely sensed data accessible from the GEE platform coupled with advanced machine learning algorithms to monitor long-term ecohydrological dynamics (over a 20-year period) of semi-permanent wetlands, using Nylsvley floodplain in Limpopo, South Africa as a case study. The findings of the study showed that the ecohydrology of the wetland varied over time and space. For example, bare surface increased twice as much as the previous measurement period, whereas short grass decreased significantly during study period 2. Moreover, the remotely sensed derived spectral indices showed similar trends throughout the 20-year period, with NDWI having minimum values less than zero in all cases implying that there was no surface inundation. However, the presence of some wetland vegetation indicated seasonal to semi-permanent soil saturation conditions. The results also showed that annual rainfall and ET were the major drivers to ecohydrological dynamics of the Nylsvley floodplain. These findings underscore the relevance of using cloud computing artificial intelligence techniques coupled with optical remotely sensed data in monitoring changes in ecohydrology of small seasonal-flooded wetlands and are critical in sustainable use and management of these systems in these regions. They provide useful alternative ways and robust methodologies to generate long term baseline information about their changes overtime - a previously daunting task from traditional mapping and monitoring techniques. This, therefore, aids in development of local to global scale frameworks that will assist in setting up conservation policies and applying effective management practices of wetlands, particularly in data scarce regions with semi-arid climates and semi-permanent wetland that vary in ecohydrology may typically be over exploited during dry periods. While the study offers new opportunities to generate high resolution continuous wetland-scale information, it is recommended that the potential of this platform in catchment-scale monitoring the impacts of adjacent land use and land cover changes as well as groundwater level change to these systems be investigated.

## Funding

The study was funded by the South African National Research Foundation (NRF) (Grant no. 131218) and the Global Monitoring for Environment and Security (GMES)—Africa through the WeMAST Project.

## CRedit authorship contribution statement

**Siyamthanda Gxokwe:** Writing – original draft. **Timothy Dube:** Conceptualization, Funding acquisition, Writing – review & editing. **Dominic Mazvimavi:** Conceptualization, Funding acquisition, Writing – review & editing. **Michael Grenfell:** Writing – review & editing.

## Declaration of Competing Interest

The authors declare that they have no known competing financial interests or personal relationships that could have appeared to influence the work reported in this paper.

## Acknowledgments

The authors would like to thank the anonymous reviewers for their valuable input to this paper as well as the Department of Earth Science, University of the Western Cape students Mr. Eugene Sagwati Maswan-ganye and Ms. Tatenda Dzurume for assisting with field data collection. The authors would also like to thank the Department of Economic Development, Environment and Tourism in Limpopo for granting access to the studied wetland.

## Appendix A. Supplementary data

Supplementary data to this article can be found online at <https://doi.org/10.1016/j.jhydrol.2022.128080>.

## References

- Achanta, R., Süsstrunk, S., 2017. Superpixels and polygons using simple non-iterative clustering. In: Proceedings - 30th IEEE Conference on Computer Vision and Pattern Recognition, CVPR 2017, pp. 4895–4904. <https://doi.org/10.1109/CVPR.2017.520>.
- African Conservation, 1998. Nylsvley Nature Reserve. Department of Environmental affairs and Tourism technical report no. 24121131313117.
- Al-Shehhi, M.R., Saffarini, R., Farhat, A., Al-Meqbali, N.K., Ghedira, H., 2011. Evaluating the effect of soil moisture, surface temperature, and humidity variations on MODIS-derived NDVI values. *Int. Geosci. Remote Sensing Symposium (IGARSS)*. 3160–3163. <https://doi.org/10.1109/IGARSS.2011.6049889>.
- Bahilu, B., Tadesse, M., 2017. Review on distribution, importance, threats and consequences of wetland degradation in Ethiopia. *Int. J. Water Resour. Environ. Eng.* 9, 64–71. <https://doi.org/10.5897/ijwree2016.0697>.
- Birkhead, A.L., James, C.S., Kleynhans, M.T., 2007. Hydrological and hydraulic modelling of the Nyl River floodplain Part 2: Modelling hydraulic behaviour. *Water SA* 33, 9–20. <https://doi.org/10.4314/wsa.v33i1.47866>.
- Blanckenberg, M., Mlambo, M.C., Parker, D., Motitsoe, S.N., Reed, C., 2020. Protected and un-protected urban wetlands have similar aquatic macroinvertebrate communities: A case study from the Cape Flats Sand Fynbos region of southern Africa. *PLoS One* 15, 1–18. <https://doi.org/10.1371/journal.pone.0233889>.
- Botai, C.M., Botai, J.O., Zwane, N.N., Hayombe, P., Wamiti, E.K., Makgoale, T., Murambadoro, M.D., Adeola, A.M., Ncongwane, K.P., de Wit, J.P., Mengistu, M.G., Tazvinga, H., 2020. Hydroclimatic extremes in the limpopo river basin, south Africa, under changing climate. *Water (Switzerland)* 12, 1–20. <https://doi.org/10.3390/w12123299>.
- Chen, Y., Qiao, S., Zhang, G., Xu, Y.J., Chen, L., Wu, L., 2020. Investigating the potential use of Sentinel-1 data for monitoring wetland water level changes in China's Momoge National Nature Reserve. *PeerJ* 2020, 1–24. <https://doi.org/10.7717/peerj.8616>.
- Dini, J., Bahadur, U., 2016. South Africa's National Wetland Rehabilitation Programme: Working for Wetlands. In: *The Wetland Book*. Springer Netherlands, pp. 1–7. [https://doi.org/10.1007/978-94-007-6172-8\\_145-2](https://doi.org/10.1007/978-94-007-6172-8_145-2).
- Dlamini, M., Adam, E., Chirima, G., Hamandawana, H., 2021a. A remote sensing-based approach to investigate changes in land use and land cover in the lower uMfolozi floodplain system, South Africa. *Trans. R. Soc. South Africa* 1–13. <https://doi.org/10.1080/0035919X.2020.1858365>.
- Dlamini, M., Chirima, G., Sibanda, M., Adam, E., Dube, T., 2021b. Characterizing leaf nutrients of wetland plants and agricultural crops with nonparametric approach using sentinel-2 imagery data. *Remote Sens.* 13, 4249. <https://doi.org/10.3390/rs13214249>.
- Dube, T., Mutanga, O., 2015. Evaluating the utility of the medium-spatial resolution Landsat 8 multispectral sensor in quantifying aboveground biomass in uMgeni catchment, South Africa. *ISPRS J. Photogramm. Remote Sens.* 101, 36–46. <https://doi.org/10.1016/j.isprsjprs.2014.11.001>.
- Dvoretz, D., Davis, C., Papez, M., 2016. Mapping and hydrologic attribution of temporary wetlands using recurrent Landsat imagery. *Wetlands* 36, 431–443. <https://doi.org/10.1007/s13157-016-0752-9>.

- Dzurume, T., Dube, T., Thamaga, K.H., Shoko, C., Mazvimavi, D., 2021. Use of multispectral satellite data to assess impacts of land management practices on wetlands in the Limpopo Transfrontier River Basin, South Africa. *South African Geogr. J.* 00, 1–20. <https://doi.org/10.1080/03736245.2021.1941220>.
- Federal Geographic Data Committee (FGDC), 1992. Application of satellite data for mapping and monitoring wetlands - fact finding report, Technical Report 1. Wetlands Subcommittee.
- Gorelick, N., Hancher, M., Dixon, M., Ilyushchenko, S., Thau, D., Moore, R., 2017. Google Earth Engine: Planetary-scale geospatial analysis for everyone. *Remote Sens. Environ.* 202, 18–27. <https://doi.org/10.1016/j.rse.2017.06.031>.
- Gxokwe, S., Dube, T., Mazvimavi, D., 2020. Multispectral remote sensing of wetlands in semi-arid and arid areas: A review on applications, challenges and possible future research directions. *Remote Sens.* 12, 1–19. <https://doi.org/10.3390/rs12244190>.
- Gxokwe, S., Dube, T., Mazvimavi, D., 2021. Leveraging Google Earth Engine platform to characterize and map small seasonal wetlands in the semi-arid environments of South Africa. *Sci. Total Environ.* 803, 150139. <https://doi.org/10.1016/j.scitotenv.2021.150139>.
- Hargreaves, G.H., Samani, Z.A., 1985. Reference Crop Evapotranspiration from Temperature. *Appl. Eng. Agric.* 1, 96–99. <https://doi.org/10.13031/2013.26773>.
- Kotze, D.C., O'connor, T.G., 2000. Vegetation Variation within and among Palustrine Wetlands along an Altitudinal Gradient. *Source Plant Ecol.* 146, 77–96.
- Kumar, L., Mutanga, O., 2018. Google Earth Engine applications since inception: Usage, trends, and potential. *Remote Sens.* 10, 1–15. <https://doi.org/10.3390/rs10101509>.
- Liu, H.Q., Huete, A., 1995. A Feedback Based Modification of the NDVI to Minimize Canopy Background and Atmospheric Noise. *IEEE Trans. Geosci. Remote Sens.* 33, 457. doi: 10.1109/TGRS.1995.8746027.
- Liu, D., Cao, C., Chen, W., Ni, X., Tian, R., Xing, X., 2017. Monitoring and predicting the degradation of a semi-arid wetland due to climate change and water abstraction in the Ordos Larus relictus National Nature Reserve, China. *Geomatics Nat. Hazards Risk* 8, 367–383. <https://doi.org/10.1080/19475705.2016.1220024>.
- Mahdianpari, M., Salehi, B., Mohammadimanesh, F., Homayouni, S., Gill, E., 2019. The first wetland inventory map of Newfoundland at a spatial resolution of 10 m using sentinel-1 and sentinel-2 data on the Google Earth Engine cloud computing platform. *Remote Sens.* 11. <https://doi.org/10.3390/rs11010043>.
- Mahdianpari, M., Salehi, B., Mohammadimanesh, F., Brisco, B., Homayouni, S., Gill, E., DeLancey, E.R., Bourgeau-Chavez, L., 2020. Big Data for a Big Country: The First Generation of Canadian Wetland Inventory Map at a Spatial Resolution of 10-m Using Sentinel-1 and Sentinel-2 Data on the Google Earth Engine Cloud Computing Platform. *Can. J. Remote Sens.* 46, 15–33. <https://doi.org/10.1080/07038992.2019.1711366>.
- Millard, K., Richardson, M., 2013. Wetland mapping with LiDAR derivatives, SAR polarimetric decompositions, and LiDAR-SAR fusion using a random forest classifier. *Can. J. Remote Sens.* 39, 290–307. <https://doi.org/10.5589/m13-038>.
- Millennium Ecosystem Assessment (Program), 2005. Ecosystems and human well-being: wetlands and water synthesis: a report of the Millennium Ecosystem Assessment. World Resources Institute. available at: <https://wedocs.unep.org/handle/20.500.11822/8735;jsessionid=9826317B1AEADDB2C8E4D2E62FECDF81>, Date accessed: 12-December-2021.
- Mosase, E., Ahiablame, L., Srinivasan, R., 2019. Spatial and temporal distribution of blue water in the Limpopo River Basin, Southern Africa: A case study. *Ecohydrol. Hydrobiol.* 19, 252–265. <https://doi.org/10.1016/j.ecohyd.2018.12.002>.
- Mudereri, B.T., Abdel-Rahman, E.M., Dube, T., Niassy, S., Khan, Z., Tonnang, H.E.Z., Landmann, T., 2021. A two-step approach for detecting Striga in a complex agroecological system using Sentinel-2 data. *Sci. Total Environ.* 762, 143151. <https://doi.org/10.1016/j.scitotenv.2020.143151>.
- Nhamo, L., Magidi, J., Dickens, C., 2017. Determining wetland spatial extent and seasonal variations of the inundated area using multispectral remote sensing. *Water SA* 43, 543–552. <https://doi.org/10.4314/wsa.v43i4.02>.
- Pande-Chhetri, R., Abd-Elrahman, A., Liu, T., Morton, J., Wilhelm, V.L., 2017. Object-based classification of wetland vegetation using very high-resolution unmanned air system imagery. *Eur. J. Remote Sens.* 50, 564–576. <https://doi.org/10.1080/22797254.2017.1373602>.
- Rebelo, L.M., 2010. Eco-Hydrological Characterization of Inland Wetlands in Africa Using L-Band SAR. *IEEE J. Sel. Top. Appl. Earth Obs. Remote Sens.* 3, 554–559. <https://doi.org/10.1109/JSTARS.2010.2070060>.
- Ryan, M.E., Palen, W.J., Adams, M.J., Rochefort, R.M., 2014. Amphibians in the climate vise: Loss and restoration of resilience of montane wetland ecosystems in the western US. *Front. Ecol. Environ.* 12, 232–240. <https://doi.org/10.1890/130145>.
- Shen, G., Yang, X., Jin, Y., Xu, B., Zhou, Q., 2019. Remote sensing and evaluation of the wetland ecological degradation process of the Zoige Plateau Wetland in China. *Ecol. Indic.* 104, 48–58. <https://doi.org/10.1016/j.ecolind.2019.04.063>.
- Simioni, J.P.D., Guasselli, L.A., de Oliveira, G.G., Ruiz, L.F.C., de Oliveira, G., 2020. A comparison of data mining techniques and multi-sensor analysis for inland marshes delineation. *Wetl. Ecol. Manag.* 28, 577–594. <https://doi.org/10.1007/s11273-020-09731-2>.
- Story, M., Congalton, R.G., 1986. *Remote Sensing Brief Accuracy Assessment: A User's Perspective*. Photogramm. Eng. Remote Sensing 52, 397–399.
- Sudmanns, M., Tiede, D., Lang, S., Bergstedt, H., Trost, G., Augustin, H., Baraldi, A., Blaschke, T., 2020. Big Earth data: disruptive changes in Earth observation data management and analysis? *Int. J. Digit. Earth* 13, 832–850. <https://doi.org/10.1080/17538947.2019.1585976>.
- Tamiminia, H., Salehi, B., Mahdianpari, M., Quackenbush, L., Adeli, S., Brisco, B., 2020. Google Earth Engine for geo-big data applications: A meta-analysis and systematic review. *ISPRS J. Photogramm. Remote Sens.* 164, 152–170. <https://doi.org/10.1016/j.isprsjprs.2020.04.001>.
- Thamaga, K.H., Dube, T., 2018. Testing two methods for mapping water hyacinth (*Eichhornia crassipes*) in the Greater Letaba river system, South Africa: discrimination and mapping potential of the polar-orbiting Sentinel-2 MSI and Landsat 8 OLI sensors. *Int. J. Remote Sens.* 39, 8041–8059. <https://doi.org/10.1080/01431161.2018.1479796>.
- Thamaga, K.H., Dube, T., Shoko, C., 2021. Advances in satellite remote sensing of the wetland ecosystems in Sub-Saharan Africa. *Geocarto Int.* 1–22. <https://doi.org/10.1080/010106049.2021.1926552>.
- Ustuner, M., Sanli, F.B., Abdikan, S., 2016. Balanced vs imbalanced training data: Classifying rapideye data with support vector machines. *Int. Arch. Photogrammetry, Remote Sens. Spatial Inf. Sci. - ISPRS Arch.* 379–384. <https://doi.org/10.5194/isprarchives-XLI-B7-379-2016>.
- van Deventer, H., Cho, M.A., Mutanga, O., 2019a. Multi-season RapidEye imagery improves the classification of wetland and dryland communities in a subtropical coastal region. *ISPRS J. Photogramm. Remote Sens.* 157, 171–187. <https://doi.org/10.1016/j.isprsjprs.2019.09.007>.
- Van Deventer, H., Smith-Adao, L., Collins, N., Grenfell, M., Grundling, A., Grundling, P.-L., Dean, I., Job, N., Dean, O., Petersen, C., Patsy, S., Erwin, S., Snaddon, K., Tererai, F., Lotter, M., Van der Collf, D., 2019. Volume 2b: Inland Aquatic (Freshwater) Realm. Report no. TT36852.
- Vlok, W., Cook, C.L., Greenfield, R., Hoare, D., Victor, J., Vuren, J.H.J. van, 2006. A BIOPHYSICAL FRAMEWORK FOR THE SUSTAINABLE MANAGEMENT OF WETLANDS IN THE LIMPOPO PROVINCE WITH Nylsvley as a reference model. Water Research Commission Report no. 1258/1/06.
- Wang, C., Chen, J., Wu, J., Tang, Y., Shi, P., Black, T.A., Zhu, K., 2017. A snow-free vegetation index for improved monitoring of vegetation spring green-up date in deciduous ecosystems. *Remote Sens. Environ.* 196, 1–12. <https://doi.org/10.1016/j.rse.2017.04.031>.
- West, H., Quinn, N., Horswell, M., White, P., 2018. Assessing vegetation response to soil moisture fluctuation under extreme drought using sentinel-2. *Water (Switzerland)* 10, 1–22. <https://doi.org/10.3390/w10070838>.
- Wetlands in Dry Lands Research Network, 2014. Parys Declaration on the Importance of Wetlands in Drylands. available at: <http://wetlandsindrylands.net/>, Date accessed: 12-December-2021.
- Wua, Q., Lane, C.R., Li, X., Zhou, K., Zhou, Y., Clinton, N., DeVries, B., Golden, H.E., Lang, M.W., 2019. Integrating LiDAR data and multi-temporal aerial imagery to map wetland inundation dynamics using Google Earth Engine. *Remote Sens. Environ.* 60, 1–24. <https://doi.org/10.1016/j.rse.2019.04.015>. Integrating.
- Xia, W., Ma, C., Liu, J., Liu, S., Chen, F., Yang, Z., Duan, J., 2019. High-resolution remote sensing imagery classification of imbalanced data using multistage sampling method and deep neural networks. *Remote Sens.* 11, 1–17. <https://doi.org/10.3390/rs11212523>.
- Zhou, Y., Dong, J., Xiao, X., Liu, R., Zou, Z., Zhao, G., Ge, Q., 2019. Continuous monitoring of lake dynamics on the Mongolian Plateau using all available Landsat imagery and Google Earth Engine. *Sci. Total Environ.* 689, 366–380. <https://doi.org/10.1016/j.scitotenv.2019.06.341>.